processes

MDPI

*Article*

# Pilot-Scale Integration of Reverse Demulsification, Coalescence and Membrane Polishing for Heavy-Crude Desalter Effluent

**Zhenyu Wang, Da Lin, Yu Lu, Meijun Liu, Bing Qin, Feng Zhang and Fan Yang ***

SINOPEC Research Institute of Petroleum Processing Co., Ltd., Beijing 100083, China
* Correspondence: yangfan29129.ripp@sinopec.com

**Abstract**

Heavy-crude desalter effluent carries a persistent oil dispersion that requires interfacial conditioning followed by engineered collection. We evaluated the cationic polyether demulsifier 6732B, dosed at 50 mg $L^{-1}$ as-received product, in a 30-day pilot campaign combining it with fiber-ball prefiltration, coated steel-mesh coalescence and modified PVDF membrane polishing at a representative external-feed set point of 0.40 $m^3$ $h^{-1}$ (nominal skid capacity, 1 $m^3$ $h^{-1}$). With matched 38,500 mg $L^{-1}$ feed, the equipment-only train left 1540 ± 73.6 mg $L^{-1}$ oil, whereas the combined train reached 13.0 ± 1.12 mg $L^{-1}$ (mean ± SD, $n = 3$), equivalent to 99.966 ± 0.003% removal ($p < 0.001$). Chemical-only bottle settling left 715 mg $L^{-1}$ after 120 min. Three replicated stage profiles located bulk oil removal at the coalescer and a low membrane-permeate endpoint. Over 30 paired days, inlet oil of 29,000–63,000 mg $L^{-1}$ was reduced to 13–38 mg $L^{-1}$ (99.94–99.96%); permeate flux was 113 ± 5.8 L $m^{-2}$ $h^{-1}$, COD after floating-oil removal decreased by 80.0 ± 2.7% and daily rinsing restored 97.1 ± 1.3% of the clean-water permeance reference. The train is a high-load de-oiling pretreatment; the remaining 400–800 mg $L^{-1}$ COD is transferred to downstream organic-pollutant treatment.

**Keywords:** desalter effluent; heavy crude oil; reverse demulsification; fibrous coalescence; membrane polishing; combined treatment; pilot-scale evaluation

## 1. Introduction

Electrostatic desalting of heavy crude produces an aqueous discharge containing dispersed oil, suspended solids and organic pollutants. Pretreatment must recover the bulk oil while suppressing the emulsified fraction carried into downstream wastewater treatment [1,2]. This separation duty is complicated by naturally occurring interfacially active components, including asphaltenes, resins and acidic species, which stabilize emulsions through interactions governed by oil and aqueous composition [3,4]. Characterization of heavy-oil desalter wastewater has identified persistent dispersed populations alongside chemically diverse polar organics [5]. High oil loading and emulsion persistence therefore impose different demands: substantial oil must be collected, and the fine dispersion must be made separable.

Coagulation destabilizes dispersed oil, with the treated-water composition reflecting both oil removal and the dissolved organics retained in the aqueous phase [6]. Heating promotes phase separation but leaves an emulsified fraction requiring further treatment [7]. Centrifugal contactors, swirling flotation with coalescing media and short-process

Academic Editor: Jorge Ancheyta

Received: 26 October 2026
Revised: 17 November 2026
Accepted: 18 November 2026
Published: 26 November 2026

**Copyright:** © 2026 by the authors. Licensee MDPI, Basel, Switzerland. This article is an open access article distributed under the terms and conditions of the Creative Commons Attribution (CC BY) license.

physical treatment have extended oil separation to industrial desalter wastewaters [8–10]. At high inlet loading, a large percentage removal can still leave substantial residual oil. The design problem is to connect interfacial destabilization to collection under flow and then retain the fraction that escapes bulk separation.

Cationic oil-in-water (O/W) demulsifiers promote association of negatively charged droplets through adsorption at their interfaces. In polymer-flooding emulsions, Bi et al. linked the action of modified hyperbranched polyamidoamines to charge neutralization and droplet growth [11]. Polyether-containing formulations add control over aqueous dispersibility and oil-interface affinity. Sun and Li showed that cationicity and the ethylene-oxide-to-propylene-oxide ratio changed charge-neutralization and interfacial-displacement functions, with different droplet-size fractions favoring different formulations [12]. Li et al. combined flexible hydrophobic chains with hydrogen-bonding sites to promote interfacial reconstruction [13]. These molecular interactions govern droplet association. A 120 min bottle endpoint includes gravity-driven migration through the water layer; the flowing bed collects conditioned oil on surfaces distributed through the stream.

Membranes retain the dispersion left after bulk collection. Ultrafiltration (UF)/reverse osmosis (RO), nanocomposite nanofiltration (NF), and serial microfiltration (MF)/UF have been investigated for desalter and oily wastewaters [14–16]. Refinery studies identify solids and colloids as sources of hydraulic resistance alongside emulsified oil [17], while ceramic-membrane experiments show that pore structure and salinity affect oil rejection and throughput differently [18]. The membrane feed therefore matters as much as the nominal separation scale: pretreatment must reduce the material deposited on the barrier while leaving it to control the final oil concentration.

Fibrous coalescers distribute oil-collecting surfaces throughout the flow. Packing geometry and superficial velocity govern droplet interception, and integration with microfiltration assigns residual-oil retention to a downstream barrier [19,20]. Physical pretreatment has also achieved joint oil and solids removal without chemical addition [21,22]. Whether chemical conditioning adds value consequently depends on the residual dispersion left by the installed equipment. Heavy-crude viscosity, interfacial stabilization and surface wetting govern droplet attachment and release [23,24]; a formulation that improves bottle separation must also produce oil entities that the collecting medium can intercept and transfer to the oil outlet.

Here, we combine 6732B conditioning with fiber-ball prefiltration, coated steel-mesh coalescence and modified PVDF membrane polishing for heavy-crude desalter effluent. Matched-feed routes determine whether chemical conditioning and physical separation together reach a water quality that either treatment leaves unattained. Interfacial measurements and droplet-size profiles connect that gain to changes in the dispersed population; stage sampling identifies where oil is collected and where the residual is retained. Adding 6732B lowered the installed-train outlet from 1540 to 13.0 mg $L^{-1}$, and a 30-day pilot series evaluated the combination under changing inlet loads. Here, "reverse demulsification" denotes destabilization of an O/W emulsion by a cationic O/W demulsifier acting on dispersed oil in the aqueous continuous phase.

## 2. Materials and Methods

### *2.1. Samples and Demulsifier*

Four desalter-effluent batches, B1–B4, were characterized as received (Table 1). B4 supplied the droplet-evolution tests and, after transfer to the pilot feed tank, the matched-route comparisons; its oil content was 37,892 mg $L^{-1}$ at characterization. The 38,500 mg $L^{-1}$ value used for the matched routes was measured at the train inlet (SP-0) after transfer of

the same batch and is the SP-0 value of stage-profile event E1 (Table S6). Prepared-emulsion screening used a separate crude-oil/injection-water sample set (Table S2).

**Table 1.** Physicochemical properties of the actual desalter-effluent characterization batches B1–B4.

| Property | Unit | B1 | B2 | B3 | B4 |
|---|---|---|---|---|---|
| Oil, raw effluent | mg $L^{-1}$ | 4127 | 9483 | 24,156 | 37,892 |
| SS, raw effluent | mg $L^{-1}$ | 719 | 1624 | 3792 | 6138 |
| COD, free-oil-removed water | mg $L^{-1}$ | 2093 | 2715 | 2947 | 3158 |
| pH | — | 8.12 | 8.03 | 7.94 | 8.05 |
| Measurement temperature | °C | 25.2 | 25.1 | 24.9 | 25.0 |
| Droplet diameter, Dv10 | μm | 3.2 | 4.9 | 5.4 | 5.5 |
| Droplet diameter, Dv50 | μm | 9.1 | 13.8 | 15.9 | 16.5 |
| Droplet diameter, Dv90 | μm | 27.3 | 38.6 | 44.5 | 41.0 |
| Oil–water density difference (25 °C) | g $cm^{-3}$ | 0.0948 | 0.1052 | 0.0879 | 0.1118 |
| Aqueous apparent viscosity (25 °C) | mPa s | 1.182 | 1.124 | 1.051 | 1.079 |
| Oil–water interfacial tension | mN $m^{-1}$ | 18.3 | 21.2 | 27.4 | 23.8 |
| Droplet zeta potential | mV | −41.8 | −35.7 | −28.3 | −32.1 |
| Electrical conductivity | μS $cm^{-1}$ | 1307 | 1294 | 1352 | 1288 |

Oil and SS were measured in raw effluent; COD was measured after floating-oil removal, which does not remove all emulsified oil. Dv10, Dv50 and Dv90 are volume-based distribution percentiles. Measurement temperature denotes the laboratory characterization temperature, not the field sampling temperature. B1–B4 are distinct from the crude-oil screening sample (Table S2). Table 1 reports the as-received batch characterization; stage-profile inlet values refer to SP-0 samples from the pilot train. — denotes a dimensionless quantity.

"Raw effluent" denotes samples before settling or floating-oil removal. Chemical oxygen demand (COD) was measured in the free-oil-removed aqueous phase. Train inlet and outlet denote SP-0 and SP-3, respectively. SS in Table 1 refers to the as-received characterization samples; stage-profile inlet SS was measured at SP-0.

6732B was a cationic polyether-containing copolymer used as an aqueous formulation. Its preparation scheme and gel permeation chromatography (GPC) profile are presented in Figure S1. Apparent $M_n$ and $M_w$ were 15,127 and 15,401 Da relative to polyethylene glycol standards (Table S1); aqueous size-exclusion chromatography settings are given in Supplementary Methods S1. The product was supplied as an aqueous concentrate and dosed on an as-received basis; its non-volatile matter, density and active-component class, and the corresponding analytical definitions are reported in Table S5. Non-volatile matter is a gravimetric specification; the active cationic copolymer content was not determined independently.

### *2.2. Bench Screening and Settling*

Bench tests assessed gravity separability (Figure 1); formulation screening used emulsions containing 50 g crude oil and 50 g injection water (Figure 2). Bench doses denote as-received product mass per total mixture mass. The dose series tested 0, 10, 25, 50, 75 and 100 μg $g^{-1}$ at 40, 60 and 80 °C. Residual oil was normalized to each temperature's zero-dose control. Comparisons at 80 °C used equal product-mass doses of 50 μg $g^{-1}$, with 10 μg $g^{-1}$ background water-in-oil (W/O) demulsifier. Supplementary treatments were the site extractant, commercial comparator or 6732B; the control received no supplementary product. The comparator was a commercially supplied polyether O/W demulsifier used at the site; its formulation was not disclosed by the supplier. Preparation details are given in Supplementary Methods S4. Mass- and volume-based product doses are related by Dv = Dmϱf, where Dm is the as-received product dose in μg $g^{-1}$ of total mixture, Dv is the

dose in mg $L^{-1}$ of feed and ϱf is the mixture density in kg $L^{-1}$; the two bases coincide numerically when ϱf is close to 1 kg $L^{-1}$. Doses are never reported on an active-ingredient basis. Supplementary Methods S1 gives the worked conversions and the basis for the oil-normalized loadings.

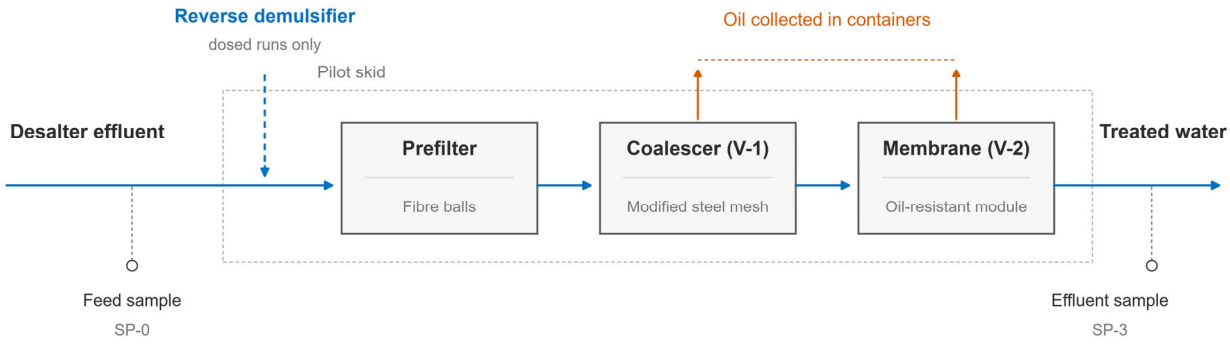
Gravity settling and bottle-route comparisons were performed at 25 ± 0.5 °C. A separate pH-response series was performed at 60 °C using independently prepared samples (Table S3). Dosed actual-effluent bottle tests of droplet evolution (Figure 3), the chemical-only route (Figure 4a) and pH response used 50 µg $g^{-1}$ 6732B per total sample mass. The principal endpoint was 120 min, with gravity settling followed to 180 min. Droplet evolution was monitored without media or equipment over 0–120 min. Independent bottles were sampled at each time point, retaining floating oil while sampling the underlying water layer (Supplementary Methods S4).

### *2.3. Treatment Train and Matched-Route Comparison*

The train comprised three serial stages: fiber-ball prefiltration, stainless-steel-mesh coalescence and membrane polishing (Scheme 1). The prefilter contained 30 L of nominally 20 mm fiber balls in a 300 mm bed. An air-actuated press plate compacted the bed during filtration and released it during backwashing.

The coalescer contained 2.0 L of 316L stainless-steel mesh with a 0.2 mm aperture, 200 mm bed height and 85% porosity. Its polysiloxane coating contained 0.2 wt% $SiO_2$.

Final polishing used a hydrophilically modified tubular poly(vinylidene fluoride) (PVDF) membrane prepared by grafting and mineralization. The module had a 25.4 mm internal diameter, 3.0 $m^2$ total effective area and 0.1 µm nominal pore size. Additional media specifications and operating details are given in Supplementary Methods S1 and S4.




**Scheme 1.** Treatment train and sampling positions. 6732B is added upstream of prefiltration in the combined route; the equipment-only route receives no supplementary chemical. Separated oil is collected from both vessels.

The same homogenized B4 feed supplied four routes: blank settling, 6732B alone, equipment alone and combined treatment. Bottle routes used 120 min settling. Both equipment routes passed through the complete prefilter–coalescer–membrane train under flow-through operation; 6732B addition distinguished the combined route. The combined route received 50 mg $L^{-1}$ as-received 6732B per feed volume. Train outlets were sampled once operating conditions had stabilized and at least one nominal residence time (2.5 h) had elapsed. Intermediate samples characterized the dosed train. The dosing pump was linked to the external-feed flow meter so that the 50 mg $L^{-1}$ set point tracked changes in feed rate.

### *2.4. Interfacial and Droplet Measurements*

Dynamic interfacial tension between recovered oil and unskimmed effluent was measured by the Wilhelmy-plate method using a K100 tensiometer (KRÜSS GmbH, Hamburg, Germany) at 25 ± 0.5 °C over 0–120 s. Background W/O treatment was common to all preparations; "no additional agent" denotes no 6732B. Each condition used three independently prepared interfaces. Instrument settings are given in Supplementary Methods S4.

Oil-droplet particle-size distributions (PSDs) were measured by laser diffraction using a Mastersizer 3000 (Malvern Panalytical Ltd., Malvern, UK). Volume-based outputs included Dv10, Dv50, Dv90 and D[4, 3]. Zeta potential was measured using a ZetaPALS analyzer (Brookhaven Instruments Corporation, Holtsville, NY, USA). Dispersion settings, optical parameters and analytical repeatability are detailed in Supplementary Methods S4.

### *2.5. Pilot Operation*

The 30-day pilot used 50 mg $L^{-1}$ as-received 6732B. External feed was adjusted cyclically to control tank level; 0.40 $m^3$ $h^{-1}$ was the representative sampling-window set point (1 $m^3$ $h^{-1}$ nominal capacity; 1.0 $m^3$ holdup). All membrane retentate returned to the feed tank. Collected oil was withdrawn every 2 h (Table S4). The 300 mg $L^{-1}$ project criterion governed transfer to downstream wastewater treatment. Operating procedures and hydraulic definitions are given in Supplementary Methods S3–S4. The demulsifier was injected upstream of prefiltration through a metering pump slaved to the external-feed signal, giving a nominal 0.050 kg of as-received product per $m^3$ of feed (20 g $h^{-1}$ at the 0.40 $m^3$ $h^{-1}$ set point). The set point was selected during commissioning, with outlet oil concentration and operating stability as the operating criteria. Two low-flow events, on days 2 and 19, are documented in Table S7; neither was removed from Figure 5.

### *2.6. Analyses, Calculations and Statistics*

Oil was measured by infrared photometry (HJ 637-2018) at low concentrations and solvent extraction–gravimetry at high loadings. COD, after floating-oil removal, was measured by rapid digestion spectrophotometry (HJ/T 399-2007), and SS gravimetrically (GB 11901-1989). Laboratory detection and reporting limits, dilution and pretreatment are detailed in Supplementary Methods S4; removal calculations are given in S2. Calibration, procedural blanks, spiked recoveries, analytical replicates, working ranges and reporting limits for oil, COD and suspended solids are summarized in Table S9. High-loading samples analyzed by extraction gravimetry and low-loading samples analyzed by infrared photometry were overlapped in the shared concentration interval to check method agreement.

For representative diameters, $d_i$, and number-weighted counts, $n_i$, the volume-weighted mean diameter was calculated as follows:

$$D[4,3] = \frac{\sum_i n_i d_i^{\,4}}{\sum_i n_i d_i^{\,3}}$$

Assuming spherical droplets, number concentration was inferred from the full volume-weighted PSD:

$$N = \frac{6C}{\pi \rho_o} \sum_i \frac{f_{v,i}}{d_i^{\,3}}$$

where C and $\varrho_o$ denote oil mass concentration and density; and $f_{v,i}$ denotes the oil-volume fraction in bin i. Figure 3c reports inferred number relative to feed. Distribution weighting is detailed in Supplementary Methods S2.

Permeate flux was calculated from measured permeate flow and the 3.0 $m^2$ area. The permeate-to-set-point flow ratio was calculated against the sampling-window external-

feed set point. Hydraulic permeance was $L_p$ = J/TMP, reported as 100 × $L_p/L_{p0}$, where $L_{p0}$ is the clean-water permeance reference, measured with deionized water on the clean membrane (Supplementary Methods S3). Vessel gauge-pressure differences in Figure 5c(ii) were recorded separately. Transmembrane pressure was calculated as TMP = (Pfeed + Pretentate)/2 − Ppermeate from the three membrane-stage gauges; it is distinct from the inter-vessel gauge-pressure difference in Figure 5c(ii). During monitored windows, TMP ranged from 0.10 to 0.14 MPa, rising before the daily rinse and returning toward the post-rinse value afterward; the clean-water reference Lp0 was 1.24 L $m^{-2}$ $h^{-1}$ $kPa^{-1}$ at 25 ± 0.5 °C and 0.10 MPa (Supplementary Methods S3, Table S4).

Bottle tests used three independently processed bottles per treatment and time point. Figure 4a reports mean ± SD for three independent bottles per bottle route and three separately collected outlet samples per continuous route. Figure 4c shows stage profile E1. Three repeated Mastersizer runs on each sample assessed analytical repeatability. Pilot averages describe temporal variation over the monitored record. Replication details are given in Supplementary Methods S4. Treatment contrasts were evaluated with a two-sided Welch's *t*-test on the three separately collected outlet samples per route ($\alpha$ = 0.05); the 30-day record was analyzed descriptively as paired daily observations from one installation. Uncertainties on derived percentages were obtained by first-order error propagation from the measured concentration SDs.

## 3. Results and Discussion

### *3.1. Feed Variability and Gravity Separability*

Oil loading varied 9.2-fold across B1–B4, from 4127 to 37,892 mg $L^{-1}$, whereas COD after floating-oil removal varied 1.5-fold, from 2093 to 3158 mg $L^{-1}$ (Table 1). SS ranged from 719 to 6138 mg $L^{-1}$, while conductivity varied from 1288 to 1352 µS $cm^{-1}$. The aqueous organic burden therefore did not increase in proportion to raw oil loading.

Volume-median droplet diameters ranged from 9.1 to 16.5 µm, with Dv90 values of 27.3–44.5 µm. Zeta potentials were negative in all four batches, ranging from −41.8 to −28.3 mV. Charged, micrometer-scale droplets therefore persisted across the measured oil-load range, making dispersion state a second determinant of separability alongside total oil concentration.

Oil concentrations fell rapidly during early settling and then approached batch-dependent residual levels above the 300 mg $L^{-1}$ project target (Figure 1a). Extending settling to 180 min did not eliminate this persistent fraction. B4 began with the highest oil loading but reached a lower long-time residual than B3, showing that initial concentration did not rank gravity separability. The 180 min size distributions were depleted in coarse droplets and enriched in the fine residual fraction (Figure 1b). This persistent dispersion is the separation duty carried forward to chemical conditioning and downstream collection.

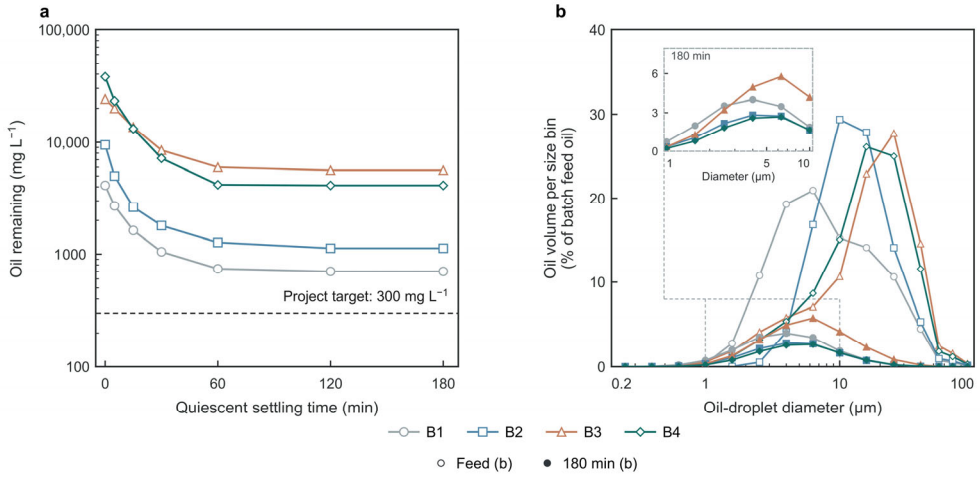



**Figure 1.** Gravity separation of batches B1–B4. (**a**) Aqueous-phase oil during settling at 25 ± 0.5 °C (mean ± SD; $n$ = 3 independent bottles); the dashed line marks the 300 mg $L^{-1}$ target. (**b**) Feed and 180 min residual PSDs, with bin oil volume relative to the initial oil volume of each batch; the inset enlarges the fine-droplet region.

### *3.2. Formulation Selection and Operating Window*

The isothermal dose responses identified a common low-residual window at 50–75 μg $g^{-1}$ (Figure 2a). Residual oil fell rapidly up to 25 μg $g^{-1}$, with smaller gains on increasing the dose to 50 μg $g^{-1}$. At that dose, residual oil relative to each temperature's zero-dose control was 0.150, 0.120 and 0.130 at 40, 60 and 80 °C, respectively. The lowest mean, 0.115, occurred at 60 °C and 75 μg $g^{-1}$.

At 100 μg $g^{-1}$, normalized residual oil rose to 0.250, 0.235 and 0.330 at 40, 60 and 80 °C, respectively, approximately 67%, 104% and 154% above the corresponding minima. Excess product therefore reversed part of the separation gain at every tested temperature. Tucker et al. measured charge reversal when poly(diallyldimethylammonium chloride) adsorbed onto sodium dodecyl sulfate (SDS)-stabilized O/W droplets: the emulsions were stable at low and high polymer concentrations and destabilized in the low-charge interval [25]. Their measurements link renewed stability to the charge of the adsorbed polymer–surfactant layer. The repeated upturn in Figure 2a places the useful 6732B window at 50–75 μg $g^{-1}$, below the excess-dose regime.

Temperature changed the residual level within that window: at 50 μg $g^{-1}$, the largest normalized residual was 25% above the smallest across 40–80 °C. In asphaltene-stabilized model O/W emulsions, Huang et al. found that heating slightly reduced branched-polyethylenimine adsorption yet promoted separation by weakening interfacial films and reducing repulsive interactions [26]. Temperature thus changes the ease of droplet association, as well as adsorption. In Figure 2a, its engineering consequence is a change in endpoint within a shared dose range; none of the three temperatures removed the penalty of dosing at 100 μg $g^{-1}$.

Under the common 10 μg $g^{-1}$ background W/O-demulsifier dose, residual oil was 2939 mg $L^{-1}$ without a supplementary product (Figure 2b). The site extractant, commercial comparator and 6732B gave 758, 864 and 268 mg $L^{-1}$, respectively. The 6732B endpoint was 90.9% below the common-background control and 69.0% below the commercial comparator, identifying it for actual-effluent and pilot evaluation. In the separate distilled-water screen, 6732B also produced the greatest separated-water volume over 10–60 min among the four conditions, including in-house candidate 6730C (Figure S2).

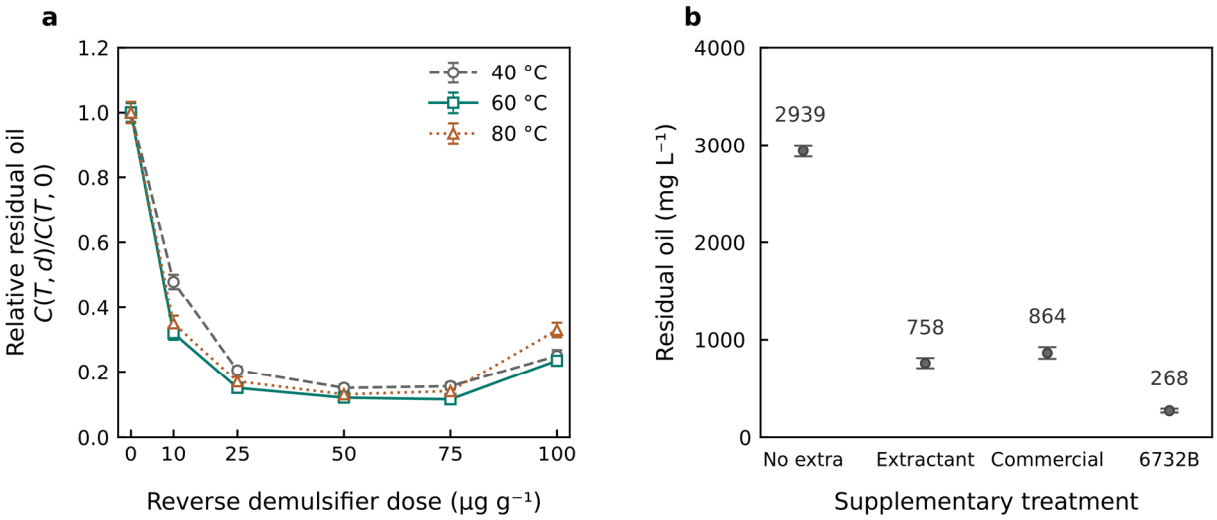



**Figure 2.** Dose selection and product screening in 1:1 crude-oil/injection-water emulsions. (**a**) Residual oil normalized to the zero-dose control at each temperature. (**b**) Residual oil after screening at 80 °C. Points and bars show mean ± SD ($n$ = 3 independent bottles). All groups contained 10 µg $g^{-1}$ background W/O demulsifier; supplementary products in (**b**) were dosed at 50 µg $g^{-1}$. Doses are as-received product per total mixture mass.

Dosed endpoints in the independent 60 °C pH series changed from 715 to 748 mg $L^{-1}$ between final pH 7.65 and 8.00, and then rose to 1032 mg $L^{-1}$ at pH 9.00, 38.0% above the pH 8.00 value (Table S3). Increased alkalinity therefore carried the larger residual-oil penalty. Havre et al. measured an apparent pKa of 4.9 for extracted naphthenic acids and showed that the electrical double layer lowers interfacial pH relative to the bulk, so bulk ionization does not fix the ionization state at the interface [27]. Brandal et al. found increasing interfacial activity from pH 5.6 to 9 for an isolated C80 tetraacid fraction [28]. These acid-interface responses explain how alkalinity can alter the adsorption environment even when bulk carboxyl groups are largely ionized. The combined route exceeded the project target at pH 10 (Figure S4), making pH control necessary alongside dose selection. Table S3 reports bottle-settling endpoints with and without 6732B, whereas Figure S4 also includes the flow-through equipment routes. The 300 mg $L^{-1}$ line is an internal project criterion for transfer to downstream wastewater treatment.

### *3.3. Interfacial Conditioning and Droplet Evolution*

Supplementary 6732B produced a larger and faster interfacial response than the common-background control (Figure 3a). From $\gamma_0$ = 24.0 mN $m^{-1}$, tension fell to 6.30 mN $m^{-1}$ at 120 s with 6732B and to 20.1 mN $m^{-1}$ without it, decreases of 73.8% and 16.2%. The measured limiting tension, $\gamma_\infty$, was 6.2 and 19.0 mN $m^{-1}$, respectively. The half-response time, $t_{1/2}$, denotes the interpolated time to half of the initial-to-limiting tension decrease (Supplementary Methods S4); it was 15.9 s with 6732B and 55.5 s for the control. The dosed interface responded within seconds and approached its limiting tension by 120 s; droplet evolution was followed over the subsequent minutes.

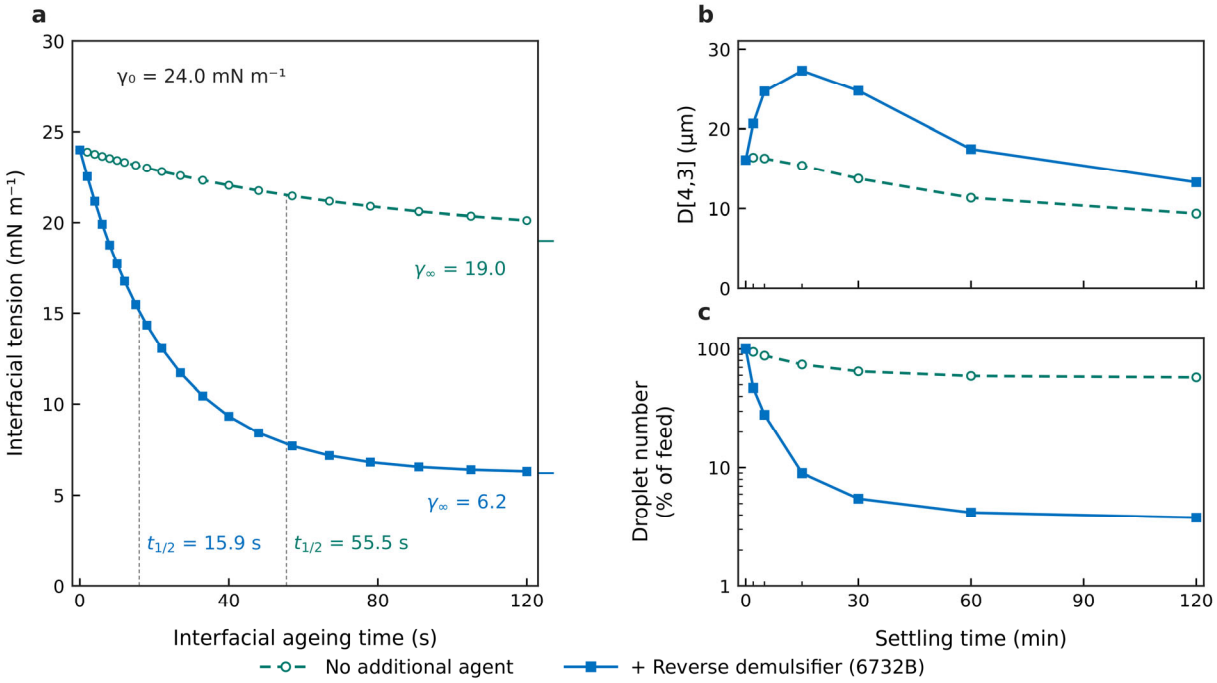



**Figure 3.** Interfacial response and droplet evolution at 25 ± 0.5 °C. (**a**) Interfacial tension ($n$ = 3 independent interfaces). (**b**) D[4, 3]. (**c**) Number inferred from PSD and residual oil, relative to feed (=100%). Dosed samples received 50 μg $g^{-1}$ 6732B per total mixture mass. Separate bottles were sampled at each time point without media, equipment or floating-oil withdrawal. Connecting lines are guides to the eye.

With 6732B, D[4, 3] increased from 16.1 to 27.3 μm at 15 min, a 70% increase, before declining to 13.3 μm at 120 min (Figure 3b). The background-only series instead decreased to 9.37 μm. Early growth distinguishes chemical conditioning from the progressive removal of coarse droplets during unassisted settling. At 120 min, inferred droplet number was 3.8% of the initial value with 6732B, versus 57.6% without additional agent, corresponding to decreases of 96.2% and 42.4% (Figure 3c). This concentration-weighted PSD metric combines the decline in dispersed oil with the redistribution of droplet sizes. Growth followed by preferential clearance of coarse oil entities leaves a finer, less concentrated residual in the sampled water layer.

The quaternary-ammonium units of 6732B provide cationic adsorption sites, while its polyether-bearing segments combine aqueous accessibility with affinity for the oil–water interface (Figure S1). The negative feed-droplet potentials, −41.8 to −28.3 mV, favor attraction of those cationic sites. Bi et al. observed that modified cationic polyamidoamines brought droplet potential close to zero and shifted oil droplets from the range of 5–35 to 30–100 μm in a polymer-flooding emulsion [11]. Sun and Li further showed that polyether–polyquaternium structure changes which droplet-size fractions respond most effectively [12]. For 6732B, the rapid tension decrease and the early size increase establish the corresponding process-level sequence: adsorption changes the interface, and the dispersed oil associates into larger entities available for collection.

Association alone leaves a transport step to be completed. At the representative 0.40 $m^3$ $h^{-1}$ external-feed setting, the mesh's 1.7 L void volume gives a 15.3 s nominal water-displacement reference (Supplementary Methods S3). The 15.9 s interfacial half-response with 6732B lies on that same seconds scale, compared with 55.5 s for the background response (Figure 3a). In a quiescent bottle, conditioned oil must migrate through the water layer under gravity. The flowing mesh places oil-collecting surfaces within the dispersion, where successive droplets encounter oil already attached to the wires. The formulation

changes the population presented to the collector; the bed collects it from moving water. The 120 min bottle endpoint and the flow-through outlet thus measure different steps in the separation. This 15.3 s value is a geometric reference derived from external flow and void volume; it is not a measured residence time inside the bed, whose internal throughflow includes recycle.

### *3.4. Chemical–Equipment Complementarity and Stage-Wise Separation*

The matched-route comparison establishes the need for both chemical conditioning and engineered collection to reach the target water quality (Figure 4a). Equipment alone removed 96.0% of oil from the common 38,500 mg $L^{-1}$ feed but left 1540 ± 73.6 mg $L^{-1}$ against the 300 mg $L^{-1}$ project target. Adding 6732B to the same train lowered the outlet to 13.0 ± 1.12 mg $L^{-1}$, 99.2% below the equipment-only outlet and equivalent to 99.97% overall removal (mean ± SD; $n$ = 3 separately collected outlet samples per route). Conversely, the chemical-only bottle route left 715 mg $L^{-1}$ after 120 min, compared with 4123 mg $L^{-1}$ for blank settling. Chemical conditioning changed the attainable water quality of the installed train, while the collecting and polishing stages removed oil that remained after chemical-only settling. The equipment-only and combined outlets differed significantly (Welch's $t$-test, $n = 3$ per route, $p < 0.001$).

The size-bin profiles reveal where the two single treatments complement one another (Figure 4b). Chemical-only treatment left less residual oil than equipment alone in the intermediate micrometer bins, whereas equipment alone left less in the coarser bins. The combined route gave the lowest residual across the resolved distribution. This crossing of the single-route profiles explains why the benefit of combination extends beyond the bulk removal percentage: each treatment acts more effectively on a different part of the residual population.

Three independent stage-sampling events under the same dosed configuration gave feed, prefilter-outlet, coalescer-outlet and membrane-permeate concentrations of 38,500 ± 400, 35,733 ± 400, 1180 ± 60 and 12.4 ± 0.7 mg $L^{-1}$, respectively (mean ± SD, $n$ = 3 events; Table S6 and Figure S5). Stage-specific concentration reductions were 7.2 ± 0.2%, 96.7 ± 0.2% and 98.946 ± 0.003%, and the coalescer accounted for 89.8 ± 0.3% of the total concentration decrease across the three events. Figure 4c shows event E1; all three events are summarized in Figure S5 and Table S6. The largest concentration decrease occurred across the coalescer; membrane polishing then set the low residual endpoint. Recorded stream volumes and estimated dry solids for one representative 8 h window are given in Table S6.

Prefiltration reduced train-inlet (SP-0) SS from 193.3 to 67.0 mg $L^{-1}$ (65.3%), with 31.8 mg $L^{-1}$ at the coalescer outlet (Figure S3).

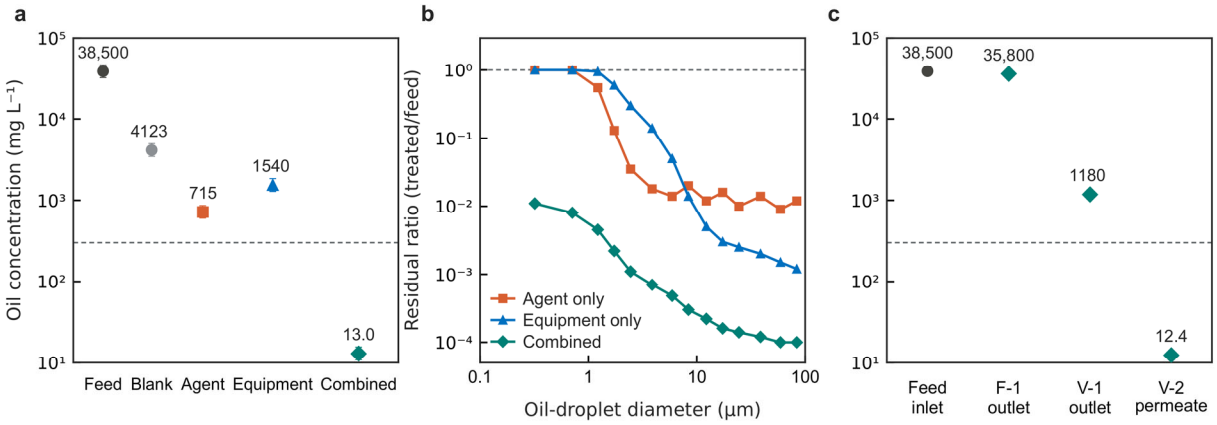


**Figure 4.** Matched-feed treatment comparison. (**a**) Route means ± SD in mg $L^{-1}$; the labels Blank, Agent, Equipment and Combined denote blank settling, 6732B-only bottle treatment, equipment-only train and combined train, respectively. Bottle routes used three independent bottles (25 ± 0.5 °C, 120 min); continuous routes used three separately collected outlet samples taken after stabilization and ≥2.5 h. Doses were 50 μg $g^{-1}$ total mixture for bottles or 50 mg $L^{-1}$ feed for the continuous train, as-received 6732B. (**b**) Size-bin residual oil relative to feed. (**c**) Dosed-train stage profile from event E1, in mg $L^{-1}$; SP-0, prefilter outlet, coalescer outlet and membrane permeate are shown in train order. The three replicated events are summarized in Figure S5 and Table S6. The common B4 feed was 38,500 mg $L^{-1}$. Dashed lines indicate the 300 mg L−1 internal pretreatment target in (**a**,**c**) and a residual ratio of 1 in (**b**).

The fiber-ball bed removed 126.3 mg $L^{-1}$ of SS before the mesh. Reducing particulate loading preserves access to collecting surfaces and the flow paths through the bed, while lowering the solids delivered to the membrane. Joint oil–solids pretreatment in refinery wastewater uses this combination of particulate filtration and fibrous collection [21,22]. Here, the 65.3% SS reduction, compared with 7.0% oil reduction, identifies solids interception as the prefilter's main duty.

The 0.2 mm mesh apertures exceed the dominant feed-droplet sizes, so oil collection depends on contact and attachment to wires rather than size exclusion [19]. The early growth in Figure 3b increases the reach of conditioned oil entities toward those surfaces. Mino et al. showed in filter simulations that wider fiber spacing permits larger collected droplets but also increases passage without coalescence [29]; attached oil and bridges between fibers extend the contact region for later droplets [30]. This creates a design trade-off between collecting opportunities and flow resistance. Yue and Mukai used hierarchical fibers to support emulsion coalescence [31], while Wu et al. obtained a higher separation quality factor with a pore-gradient stack than with a uniform fine-pore stack by balancing collection against pressure loss [32]. The mesh therefore supplies repeated surface encounters without requiring every flow passage to be smaller than the incoming droplets.

Oil growth on the wires must be followed by release to sustain collection. Buoyancy increases with the volume of an attached oil entity, while capillary retention acts along its contact region with the wire; flow and buoyancy eventually detach the enlarged entity. Work on microbubble-assisted O/W coalescers and fibrous filter-coalescers for bitumen emulsions links droplet detachment to renewal of the collecting surface [33,34]. In the present train, the separated oily phase was withdrawn from both vessels every 2 h into 20 L sealed containers. Each two-hour drain produced 30–50 L, including associated emulsified water, transferring the collected phase out of the treatment stream.

The PVDF membrane retains the dispersion remaining after bulk collection. Hydrophilic modification favors water wetting; displacing water associated with the surface imposes an energetic cost on direct oil–polymer contact, as demonstrated for hydration-reinforced PVDF [35]. Water passes through the wetted 0.1 μm pores, whereas an approaching oil droplet must deform and displace that water to enter. Retention therefore combines pore geometry with the capillary barrier set by interfacial tension and wetting.

Lowering IFT eases pressure-driven oil deformation, so the membrane response cannot be inferred from the tension decrease alone [36]. Virga et al. found that lowering IFT reduced oil retention for three surfactant systems on silicon-carbide membranes, whereas a zwitterionic system retained oil at low IFT, demonstrating the joint importance of interfacial tension and membrane wetting [37]. In the dosed profile here, upstream collection reduced oil from 38,500 to 1180 mg $L^{-1}$ before the membrane; polishing then reduced that residual by 98.9% to 12.4 mg $L^{-1}$. This arrangement places bulk collection ahead of the pore-entry barrier and limits the oil population that reaches it. Coalescer–

microfiltration experiments similarly show how upstream oil removal supports membrane throughput [20]. The chemical step promotes association, the mesh collects the bulk oil and the water-wetted membrane sets the final residual concentration.

### *3.5. Thirty-Day Performance and Maintainability*

Inlet oil varied from approximately 29,000 to 63,000 mg $L^{-1}$, a 2.2-fold range, across the full 30-day pilot series (Figure 5a). Treated-water oil ranged from approximately 13 to 38 mg $L^{-1}$ and remained below the 300 mg $L^{-1}$ project criterion throughout the monitored record. Paired inlet–outlet concentrations corresponded to reductions of 99.94–99.96%. The paired inlet and outlet values are listed in Table S10; the range describes 30 daily records from one installation.

The 50 mg $L^{-1}$ product-dose set point was maintained across this 2.2-fold inlet-oil range, and stable outlet quality at that fixed dose demonstrates load tolerance of the installed combination. At 38,500 mg $L^{-1}$ inlet oil, 50 mg $L^{-1}$ corresponds to approximately 1300 mg of as-received product per kg of oil, compared with 100–150 mg $kg^{-1}$ for the 50–75 μg $g^{-1}$ screening window in the 50 wt% oil emulsion. The actual-effluent bottle tests used 50 μg $g^{-1}$ of total sample, approximately 50 mg $L^{-1}$ at a feed density near 1 kg $L^{-1}$, and therefore applied a similar oil-normalized loading at the matched-feed concentration. Because the dosing pump tracked external-feed flow, the as-received product consumption was nominally 0.050 kg per $m^3$ of feed across the load range, equivalent to 20 g $h^{-1}$ at the representative set point; the oil-normalized loading consequently varied from approximately 790 to 1720 mg $kg^{-1}$ oil as inlet oil changed.

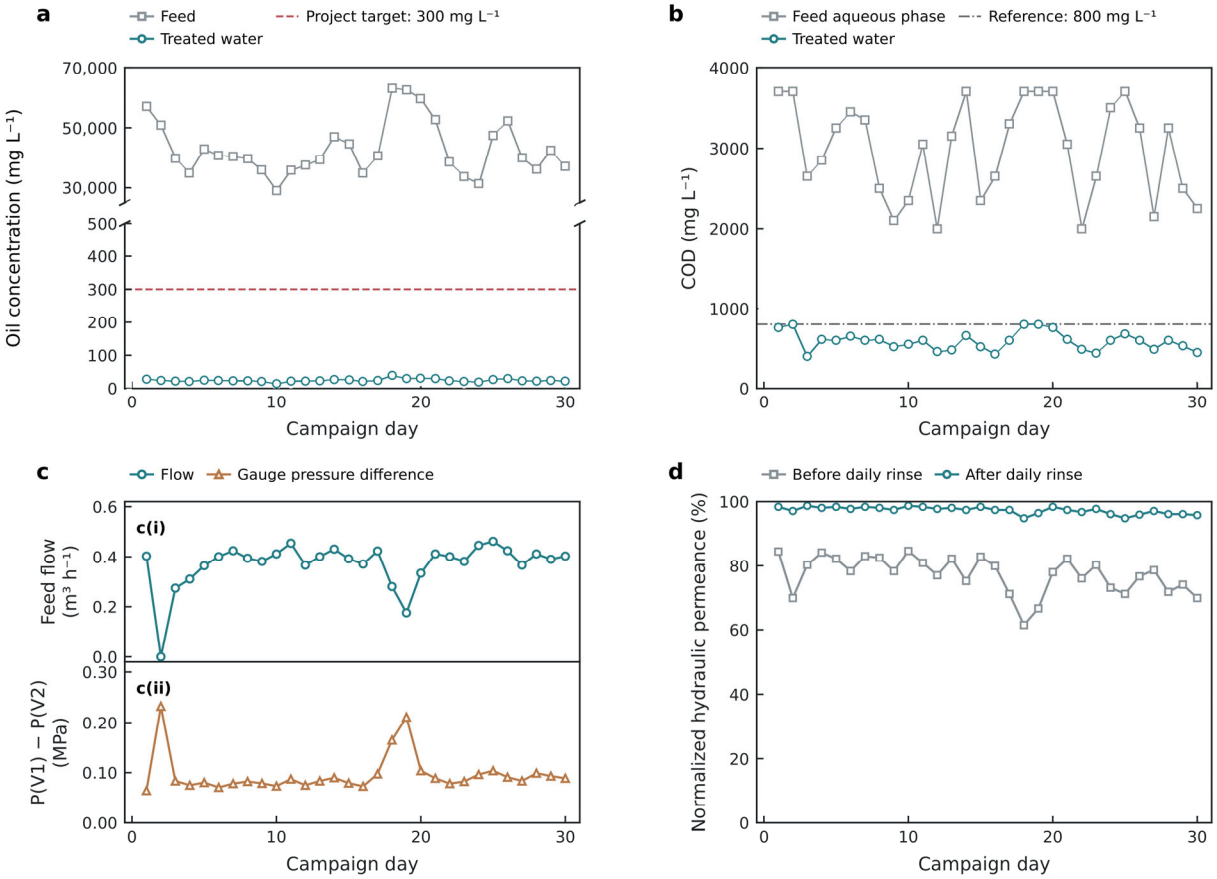



**Figure 5.** Thirty-day pilot operation. (**a**) Inlet and treated-water oil in mg $L^{-1}$; the dashed line marks the 300 mg $L^{-1}$ internal pretreatment target. (**b**) COD after floating-oil removal in mg $L^{-1}$; 800 mg $L^{-1}$ is an internal operating reference, not a discharge limit. (**c**) Separate traces of (i) feed flow in $m^3$ $h^{-1}$ and (ii) coalescence–membrane vessel gauge-pressure difference, P(V1)–P(V2), in MPa; this inter-

vessel difference is not the membrane TMP. (**d**) Normalized membrane permeance, 100 × Lp/Lp0, before and after daily rinsing; corresponding permeate flux ranged from 108 to 121 L $m^{-2}$ $h^{-1}$. SD values in the text describe temporal variation over the monitored record. Campaign day includes commissioning and interruptions; low-flow events on days 2 and 19 are identified in Table S7.

Aqueous-phase COD decreased from a range of approximately 2000–3700 mg $L^{-1}$ at the inlet to a range of 400–800 mg $L^{-1}$ after treatment, with paired reductions of 75–85% (Figure 5b). Both series used floating-oil removal before analysis. For comparison, the 13–38 mg $L^{-1}$ residual oil corresponds to about 39–133 mg $L^{-1}$ oxygen demand on a hydrocarbon stoichiometric basis (Supplementary Methods S2). Oil alone therefore does not account for the remaining COD. The polar dissolved organics and colloidal material identified in heavy-oil desalter wastewaters [5] explain why downstream treatment must address an organic load that persists after efficient de-oiling. Over the paired record, outlet COD averaged 590 ± 114 mg $L^{-1}$ with reductions of 80.0 ± 2.7%. The train therefore removes the high oil load before downstream treatment of the remaining organic pollutants.

Mean membrane flux during the monitored operating windows was 113 ± 5.8 L $m^{-2}$ $h^{-1}$. Relative to the 0.40 $m^3$ $h^{-1}$ external-feed set point, permeate production was 84.8 ± 4.4%; representative cycle conditions spanned 108–121 L $m^{-2}$ $h^{-1}$ and 81.0–90.5%, respectively (Table S4). External feed was adjusted over the cycle to control tank level, with membrane retentate returned to the feed tank. Feed flow recovered to approximately 0.40 $m^3$ $h^{-1}$ by day 6 after a zero-flow reading on day 2, and from 0.18 $m^3$ $h^{-1}$ on day 19 to 0.41 $m^3$ $h^{-1}$ on day 21 (Figure 5c(i)). The inter-vessel gauge-pressure difference reached approximately 0.23 MPa on day 2 and 0.21 MPa on day 19 (Figure 5c(ii)). Normalized membrane permeance was approximately 61–85% before daily rinsing and returned to 95–99% afterward (Figure 5d). During the monitored windows the membrane-stage TMP ranged from 0.10 to 0.14 MPa, rising with deposited oil before the daily rinse and returning close to the post-rinse value afterward (Table S4). The day-2 and day-19 low-flow events are logged in Table S7. Cleaning was hydraulic only: a daily forward water rinse with temperature-controlled water, with periodic hot-water flushing to support restart. Rinsing restored 97.1 ± 1.3% of the clean-water permeance reference. No membrane replacement was required during the 30-day campaign. For extended operation, replacement should be considered when appropriate cleaning no longer restores the required throughput or permeate quality, or when membrane integrity is compromised.

Daily rinsing restored hydraulic performance throughout the 30-day campaign. Hydrated PVDF surfaces resist direct oil attachment [35,38], while hydraulic removal of deposited material restores flow paths, as observed in oily-water filtration and cleaning studies [39,40]. The record supports short-term maintainability; it does not establish membrane service life or quantify irreversible fouling.

Centrifugal contactors treated 4000–60,000 mg $L^{-1}$ oil to below 200 mg $L^{-1}$ under optimized conditions [8], and swirling flotation with medium coalescence stabilized effluent oil below 30 mg $L^{-1}$ from feeds in the range of 400–2500 mg $L^{-1}$ [9]. The present train treated 29,000–63,000 mg $L^{-1}$ inlet oil to 13–38 mg $L^{-1}$ outlet oil while allowing repeated permeance recovery on the same installation.

At the site product price of 28 CNY $kg^{-1}$, the 0.050 kg $m^{-3}$ dose contributed 1.40 CNY $m^{-3}$, about half of the estimated subtotal. That subtotal, 2.9 CNY $m^{-3}$ of feed, covers demulsifier, rinse make-up water, pump electricity and steam for hot-water rinsing (Table S12); Table S11 lists the operating consumptions and compares reported inlet and outlet oil concentrations with centrifugation [8] and swirling flotation [9]. The estimate is a screening calculation that combines dose-based chemical consumption and campaign-averaged make-up water with site unit prices and reference electricity and steam scenarios;

it excludes capital, labor, maintenance, membrane and media replacement, and waste management.

## 4. Conclusions

6732B and the three-stage train performed complementary separation duties. In bench bottle tests, chemical-only settling left 715 mg $L^{-1}$ after 120 min; in the continuous matched-route comparison, the equipment-only train left 1540 ± 73.6 mg $L^{-1}$, and the combined train reached 13.0 ± 1.12 mg $L^{-1}$, equivalent to 99.966 ± 0.003% removal (Welch's *t*-test, $p < 0.001$). The 15.9 s interfacial half-response and the mesh's 15.3 s nominal water-displacement reference place chemical conditioning and collector hydraulics on a common seconds scale; D[4, 3] rose 70% within 15 min. The crossing single-route size-bin profiles show why neither treatment alone controls the full residual population. Across three replicated dosed stage profiles, the largest concentration decrease occurred at the coalescer, after which the membrane set the low-oil endpoint. Chemical conditioning thus improves the dispersion presented for collection, and successive physical stages convert that change into treated-water quality.

Across the 30-day record from one installation, outlet oil remained at 13–38 mg $L^{-1}$ with paired reductions of 99.94–99.96% under changing inlet loads. Permeate flux was 113 ± 5.8 L $m^{-2}$ $h^{-1}$, and daily rinsing restored 97.1 ± 1.3% of the clean-water permeance reference, allowing repeated operation of the polishing stage. Aqueous COD decreased by 80.0 ± 2.7%, with 400–800 mg $L^{-1}$ remaining for downstream organic-pollutant treatment. The combination provides high-load de-oiling through an explicit sequence of interfacial conditioning, bulk collection and residual retention, with periodic withdrawal of a recoverable oily stream.

**Supplementary Materials:** The following supporting information can be downloaded at https://www.mdpi.com/article/10.3390/pr14233819/s1: Supplementary Methods S1. Formulation architecture and separation media. Table S1. Apparent molecular-mass parameters of the integrated 6732B GPC peak. Figure S1. Preparation scheme and GPC characterization of 6732B. (a) Polyether precursor formation, methacrylate functionalization and copolymerization with MMA and DAC. A and B label intermediates; m, n and p label schematic repeat units. Figure S1 continued. (b) GPC profile of 6732B. The marked peak has Mp = 15,440 Da; Table S1 reports the molecular-mass statistics for this integrated peak. Supplementary Methods S2. Removal metrics and droplet calculations. Supplementary Methods S3. Hydraulic calculations. Table S4. Representative membrane operating conditions at an external-feed set point of 0.40 $m^3$ $h^{-1}$ and a membrane area of 3.0 $m^2$. Supplementary Methods S4. Experimental procedures and analytical settings. Table S2. Properties of the heavy crude oil used for the prepared-emulsion screening. Table S3. Residual-oil endpoints in the independent pH-response series at 60 °C and 120 min, mean ± SD of n = 3 independent bottles. Each row compares no-additional-agent and 6732B-treated samples at the same final pH. The dose was 50 μg $g^{-1}$ of total sample mass, as-received product. These are bottle endpoints; complete-train performance is reported in Figure 4a and Figure 5a of the main text. Figure S2. Preliminary screening in 1:1 crude-oil/distilled-water emulsions at 80 °C: separated-water volume (mL) during 10–60 min settling. All groups contained 10 μg $g^{-1}$ W/O demulsifier; supplementary products were dosed at 50 μg $g^{-1}$ total mixture. The in-house candidate 6730C differs from the commercial comparator in Figure 2b. Figure S3. Suspended solids in mg $L^{-1}$ at the train inlet (SP-0) and after prefiltration, coalescence and membrane treatment in the dosed route, mean ± SD of three independent stage-sampling events (Table S6). ND denotes a value below the 5 mg $L^{-1}$ laboratory practical reporting limit; error bars denote SD of the independent events. Figure S4. pH response of the four treatment routes at 60 °C. Bottle routes (blank settling and 6732B-only bottle treatment) were held for 120 min; points are means of n = 3 independent bottles per condition; the matched final-pH bottle endpoints at pH 7.65, 8.00 and 9.00 are listed in Table S3. Only the 6732B-only bottle route received 50 μg $g^{-1}$

6732B per total mixture mass; blank settling received none. Equipment-platform endpoints are samples collected during stabilized operating windows of the continuous train at 0.40 $m^3$ $h^{-1}$ with full retentate recycle and 50 mg $L^{-1}$ dosing in the combined route, taken after ≥ 2.5 h of stabilized operation; these are controlled-pH platform comparisons. Points on the equipment routes show means of n = 3 separately collected outlet samples per route. The dashed line marks the 300 mg $L^{-1}$ internal project target; connecting lines are guides to the eye. Supplementary Methods S5. Product specification and residual demulsifier. Table S5. Specification of the as-received 6732B formulation. Supplementary Methods S6. Replicated stage profiles and stream-volume records. Table S6. Replicated dosed stage profiles and recorded stream volumes. Table S6 (continued). Recorded stream volumes and estimated solids for a representative 8 h window. Figure S5. Replicated dosed-train stage profiles. Oil concentration in mg $L^{-1}$ at SP-0, prefilter outlet, coalescer outlet and membrane permeate for three independent sampling events; symbols show individual events and the bars show mean ± SD (n = 3). Numerical values are given in Table S6. Supplementary Methods S7. Statistical definitions and QA/QC. Table S7. Low-flow events and operating responses. Table S8. Replication levels and the statistical object of each reported SD. Table S9. Analytical QA/QC summary. Table S10. Daily paired pilot records (oil and COD in mg $L^{-1}$). Supplementary Methods S8. Operating consumption, cost items and process comparison. Table S11. Resource inventory and screening-level process comparison. Table S11 (continued). Comparison of reported inlet load and outlet quality. Table S12. Preliminary operating cost items per $m^3$ of feed. References [41,42] are cited in the supplementary materials.

**Author Contributions:** Conceptualization, F.Y.; methodology, Y.L., F.Y. and F.Z.; investigation, Z.W., D.L., Y.L., M.L. and B.Q.; validation, D.L.; formal analysis, Z.W.; data curation, Z.W. and M.L.; resources, B.Q.; writing—original draft preparation, Z.W.; writing—review and editing, F.Y. and F.Z.; supervision, F.Z. and F.Y.; project administration, F.Z.; funding acquisition, F.Y. All authors have read and agreed to the published version of the manuscript.

**Funding:** This research was funded by China Petroleum & Chemical Corporation (SINOPEC) (Grant Nos. CLY23068 and 126012_2).

**Data Availability Statement:** The data that support the findings of this study are available from the corresponding author upon reasonable request; the raw data are not publicly available owing to commercial confidentiality agreements with SINOPEC, and may be provided with institutional approval.

**Conflicts of Interest:** Authors Zhenyu Wang, Da Lin, Yu Lu, Meijun Liu, Bing Qin, Feng Zhang and Fan Yang were employed by the company SINOPEC Research Institute of Petroleum Processing Co., Ltd. The authors declare that this study received funding from China Petroleum & Chemical Corporation (SINOPEC). The funder was not involved in the study design, collection, analysis, interpretation of data, the writing of this article or the decision to submit it for publication.

## References

1. Abuhasel, K.; Kchaou, M.; Alquraish, M.; Munusamy, Y.; Jeng, Y.T. Oily Wastewater Treatment: Overview of Conventional and Modern Methods, Challenges, and Future Opportunities. *Water* **2021**, *13*, 980. https://doi.org/10.3390/w13070980.
2. Medeiros, A.D.M.d.; Silva Junior, C.J.G.d.; Amorim, J.D.P.d.; Durval, I.J.B.; Costa, A.F.d.S.; Sarubbo, L.A. Oily Wastewater Treatment: Methods, Challenges, and Trends. *Processes* **2022**, *10*, 743. https://doi.org/10.3390/pr10040743.
3. Wang, D.; Yang, D.; Huang, C.; Huang, Y.; Yang, D.; Zhang, H.; Liu, Q.; Tang, T.; Gamal El-Din, M.; Kemppi, T.; et al. Stabilization Mechanism and Chemical Demulsification of Water-in-Oil and Oil-in-Water Emulsions in Petroleum Industry: A Review. *Fuel* **2021**, *286*, 119390. https://doi.org/10.1016/j.fuel.2020.119390.
4. Ma, J.; Yao, M.; Yang, Y.; Zhang, X. Comprehensive Review on Stability and Demulsification of Unconventional Heavy Oil-Water Emulsions. *J. Mol. Liq.* **2022**, *350*, 118510. https://doi.org/10.1016/j.molliq.2022.118510.

5. Ye, H.; Liu, B.; Wang, Q.; How, Z.T.; Zhan, Y.; Chelme-Ayala, P.; Guo, S.; Gamal El-Din, M.; Chen, C. Comprehensive Chemical Analysis and Characterization of Heavy Oil Electric Desalting Wastewaters in Petroleum Refineries. *Sci. Total Environ.* **2020**, *724*, 138117. https://doi.org/10.1016/j.scitotenv.2020.138117.
6. Ye, H.; Chen, L.; Kou, Y.; How, Z.T.; Chelme-Ayala, P.; Wang, Q.; An, Z.; Guo, S.; Chen, C.; Gamal El-Din, M. Influences of Coagulation Pretreatment on the Characteristics of Crude Oil Electric Desalting Wastewaters. *Chemosphere* **2021**, *264*, 128531. https://doi.org/10.1016/j.chemosphere.2020.128531.
7. Zhang, H.; Wang, Z.S.; Li, J.F.; Li, M.X.; Zhang, Z.J.; Song, J.Y.; Wang, Y.L. Characterization of Desalting Wastewater: Stability and Demulsification Mechanisms. *J. Water Process Eng.* **2025**, *76*, 108296. https://doi.org/10.1016/j.jwpe.2025.108296.
8. Hao, M.; Bai, Z.; Wang, H.; Liu, W. Removal of Oil from Electric Desalting Wastewater Using Centrifugal Contactors. *J. Pet. Sci. Eng.* **2013**, *111*, 37–41. https://doi.org/10.1016/j.petrol.2013.10.017.
9. Wu, S.A.; Liu, Y.Q.; Pan, Z.C.; Dai, P.Y.; Yang, Q.; Lu, H. Treatment of Electric Desalting Wastewater by Swirling Flotation Coupled with Medium Coalescence. *J. Environ. Chem. Eng.* **2021**, *9*, 106055. https://doi.org/10.1016/j.jece.2021.106055.
10. Li, B.H.; Li, S.X.; Li, Y.; Liu, H.N.; Huang, S.; Yang, Q.; Liu, Y.Q. Pilot Test Study on a New Physical Treatment Method for the Electric Desalting Wastewater. *J. Environ. Sci.* **2025**, *156*, 806–820. https://doi.org/10.1016/j.jes.2024.10.034.
11. Bi, Y.; Tan, Z.; Wang, L.; Li, W.; Liu, C.; Wang, Z.; Liu, X.; Jia, X. The Demulsification Properties of Cationic Hyperbranched Polyamidoamines for Polymer Flooding Emulsions and Microemulsions. *Processes* **2020**, *8*, 176. https://doi.org/10.3390/pr8020176.
12. Sun, H.; Li, X. Enhanced Demulsification of Alkaline-Surfactant-Polymer Flooding O/W Emulsion by Multibranched Polyether-Polyquaternium Based on the Size Effect of Oil Droplets. *Chemosphere* **2024**, *363*, 142768. https://doi.org/10.1016/j.chemosphere.2024.142768.
13. Li, Z.; Zhang, B.; Zhao, Y.; Chen, L.; Jin, B.; Ding, Y.; Ma, W.; Mi, Y.; Li, H. Synthesis of a Highly Efficient Demulsifier for Oil-in-Water Emulsions via Low Temperature Two-Step Route. *Colloids Surf. A Physicochem. Eng. Asp.* **2026**, *738*, 140008. https://doi.org/10.1016/j.colsurfa.2026.140008.
14. Norouzbahari, S.; Roostaazad, R.; Hesampour, M. Crude Oil Desalter Effluent Treatment by a Hybrid UF/RO Membrane Separation Process. *Desalination* **2009**, *238*, 174–182. https://doi.org/10.1016/j.desal.2008.01.045.
15. Dadari, S.; Rahimi, M.; Zinadini, S. Crude Oil Desalter Effluent Treatment Using High Flux Synthetic Nanocomposite NF Membrane-Optimization by Response Surface Methodology. *Desalination* **2016**, *377*, 34–46. https://doi.org/10.1016/j.desal.2015.09.005.
16. Masoudnia, K.; Raisi, A.; Aroujalian, A.; Fathizadeh, M. A Hybrid Microfiltration/Ultrafiltration Membrane Process for Treatment of Oily Wastewater. *Desalin. Water Treat.* **2015**, *55*, 901–912. https://doi.org/10.1080/19443994.2014.922501.
17. Madaeni, S.S.; Gheshlaghi, A.; Rekabdar, F. Membrane Treatment of Oily Wastewater from Refinery Processes. *Asia-Pac. J. Chem. Eng.* **2013**, *8*, 45–53. https://doi.org/10.1002/apj.1619.
18. Rasouli, Y.; Parivazh, M.M.; Abbasi, M.; Akrami, M. The Effect of Ceramic Membranes' Structure on the Oil and Ions Removal in Pre-Treatment of the Desalter Unit Wastewater. *Membranes* **2022**, *12*, 59. https://doi.org/10.3390/membranes12010059.
19. Lu, H.; Yang, Q.; Xu, X.; Wang, H.-L. Effect of the Mixed Oleophilic Fibrous Coalescer Geometry and the Operating Conditions on Oily Wastewater Separation. *Chem. Eng. Technol.* **2016**, *39*, 255–262. https://doi.org/10.1002/ceat.201400773.
20. Motta, A.; Borges, C.; Esquerre, K.; Kiperstok, A. Oil Produced Water Treatment for Oil Removal by an Integration of Coalescer Bed and Microfiltration Membrane Processes. *J. Membr. Sci.* **2014**, *469*, 371–378. https://doi.org/10.1016/j.memsci.2014.06.051.
21. Li, Y.; Lu, H.; Liu, Y.; Dai, P.; Zhu, H.; Zhang, B.; Peng, S.; Fan, Y.; Yang, Q. Media Coalescence Filtration as a Novel Method for Pretreatment of Refinery Wastewater. *J. Environ. Chem. Eng.* **2023**, *11*, 109107. https://doi.org/10.1016/j.jece.2022.109107.
22. Sun, Y.; Liu, Y.; Chen, J.; Huang, Y.; Lu, H.; Yuan, W.; Yang, Q.; Hu, J.; Yu, B.; Wang, D.; et al. Physical Pretreatment of Petroleum Refinery Wastewater Instead of Chemicals Addition for Collaborative Removal of Oil and Suspended Solids. *J. Clean. Prod.* **2021**, *278*, 123821. https://doi.org/10.1016/j.jclepro.2020.123821.
23. Jiang, X.; Yang, F.C.; Guo, Z.G. Superwetting Surfaces for Filtration Separation of High-Viscosity Raw Petroleum/Water Mixtures. *J. Mater. Chem. A* **2022**, *10*, 14273–14292. https://doi.org/10.1039/d2ta03444a.
24. Munirasu, S.; Haija, M.A.; Banat, F. Use of Membrane Technology for Oil Field and Refinery Produced Water Treatment—A Review. *Process Saf. Environ. Prot.* **2016**, *100*, 183–202. https://doi.org/10.1016/j.psep.2016.01.010.
25. Tucker, I.M.; Petkov, J.T.; Jones, C.; Penfold, J.; Thomas, R.K.; Rogers, S.E.; Terry, A.E.; Heenan, R.K.; Grillo, I. Adsorption of Polymer–Surfactant Mixtures at the Oil–Water Interface. *Langmuir* **2012**, *28*, 14974–14982. https://doi.org/10.1021/la303563j.

26. Huang, Y.; Qiao, C.; Li, Z.; Zeng, H. Mechanistic insights into the role of branched polyethylenimine in breaking Asphaltene-Stabilized Oil-in-Water emulsions: Temperature effects. *Sep. Purif. Technol.* **2025**, *362*, 131913. https://doi.org/10.1016/j.seppur.2025.131913.
27. Havre, T.E.; Sjöblom, J.; Vindstad, J.E. Oil/Water-Partitioning and Interfacial Behavior of Naphthenic Acids. *J. Dispers. Sci. Technol.* **2003**, *24*, 789–801. https://doi.org/10.1081/dis-120025547.
28. Brandal, Ø.; Hanneseth, A.D.; Hemmingsen, P.V.; Sjöblom, J.; Kim, S.; Rodgers, R.P.; Marshall, A.G. Isolation and Characterization of Naphthenic Acids from a Metal Naphthenate Deposit: Molecular Properties at Oil-Water and Air-Water Interfaces. *J. Dispers. Sci. Technol.* **2006**, *27*, 295–305. https://doi.org/10.1080/01932690500357909.
29. Mino, Y.; Hasegawa, A.; Shinto, H.; Matsuyama, H. Lattice-Boltzmann Flow Simulation of an Oil-in-Water Emulsion through a Coalescing Filter: Effects of Filter Structure. *Chem. Eng. Sci.* **2018**, *177*, 210–217. https://doi.org/10.1016/j.ces.2017.11.027.
30. Mino, Y.; Kagawa, Y.; Matsuyama, H.; Ishigami, T. Permeation of Oil-in-water Emulsions through Coalescing Filter: Two-dimensional Simulation Based on Phase-field Model. *AIChE J.* **2016**, *62*, 2525–2532. https://doi.org/10.1002/aic.15206.
31. Yue, Y.; Mukai, Y. Electrospun Hierarchically Structured Nanofibrous Membrane for Highly Efficient Oil-in-Water Emulsion Coalescence Separation. *Sep. Purif. Technol.* **2023**, *322*, 124331. https://doi.org/10.1016/j.seppur.2023.124331.
32. Wu, X.; Wang, Y.; Li, C.; Liu, L.; Li, X.; Chang, C. Multi-Layer Filter Material with a Superoleophobic Pore Size Gradient for the Coalescence Separation of Surfactant-Stabilized Oil-in-Water Emulsions. *Processes* **2025**, *13*, 1600. https://doi.org/10.3390/pr13051600.
33. Li, Y.; Jiang, H.; Wu, Y.; Zhu, H.; Liu, Y.; Lu, H.; Liu, B.; Yang, Q. Microbubbles Enhance Oil-in-Water Emulsion Separation in Fibrous Coalescers. *Water Res.* **2025**, *268*, 122573. https://doi.org/10.1016/j.watres.2024.122573.
34. Ajogbeje, O.J.; Stammitti-Scarpone, A.; Cao, S.; Akanni, T.; Ng, S.; Acosta, E.J. Separation of Emulsions with Fibrous Filter-Coalescers. *Langmuir* **2021**, *37*, 7630–7642. https://doi.org/10.1021/acs.langmuir.1c00333.
35. Xiong, Z.; He, Z.; Mahmud, S.; Yang, Y.; Zhou, L.; Hu, C.; Zhao, S. Simple Amphoteric Charge Strategy to Reinforce Superhydrophilic Polyvinylidene Fluoride Membrane for Highly Efficient Separation of Various Surfactant-Stabilized Oil-in-Water Emulsions. *ACS Appl. Mater. Interfaces* **2020**, *12*, 47018–47028. https://doi.org/10.1021/acsami.0c13508.
36. Tanudjaja, H.J.; Hejase, C.A.; Tarabara, V.V.; Fane, A.G.; Chew, J.W. Membrane-Based Separation for Oily Wastewater: A Practical Perspective. *Water Res.* **2019**, *156*, 347–365. https://doi.org/10.1016/j.watres.2019.03.021.
37. Virga, E.; Bos, B.; Biesheuvel, P.M.; Nijmeijer, A.; Vos, W.M. Surfactant-dependent critical interfacial tension in silicon carbide membranes for produced water treatment. *J. Colloid Interface Sci.* **2020**, *571*, 222–231. https://doi.org/10.1016/j.jcis.2020.03.032.
38. Alrasheedi, N.F.H.; Abdulazeez, I.; Baig, N.; Salhi, B.; Asmaly, H.A.; Haladu, S.A.; Elsharif, A.M. Antifouling Macrocyclic-Engineered PVDF Membrane for the Low-Pressure Separation of Surfactant-Stabilized Oily Wastewater. *J. Environ. Chem. Eng.* **2024**, *12*, 112850. https://doi.org/10.1016/j.jece.2024.112850.
39. Sutrisna, P.D.; Kurnia, K.A.; Siagian, U.W.R.; Ismadji, S.; Wenten, I.G. Membrane Fouling and Fouling Mitigation in Oil–Water Separation: A Review. *J. Environ. Chem. Eng.* **2022**, *10*, 107532. https://doi.org/10.1016/j.jece.2022.107532.
40. Zhu, X.; Dudchenko, A.; Gu, X.; Jassby, D. Surfactant-Stabilized Oil Separation from Water Using Ultrafiltration and Nanofiltration. *J. Membr. Sci.* **2017**, *529*, 159–169. https://doi.org/10.1016/j.memsci.2017.02.004. Correction in *J. Membr. Sci.* **2017**, *523*, 969.
41. Wang, S.; Liu, C.; Li, Q. Impact of polymer flocculants on coagulation-microfiltration of surface water. *Water Res.* **2013**, *47*, 4538–4546. https://doi.org/10.1016/j.watres.2013.04.040.
42. Salinas, E.R.; Bozich, J.S.; Kolbenschlag, S.; Kary-Heinrich, M.; Hopp, P.W.; Lukas, R.; Zok, S.; Hidding, B. Aquatic testing guidelines insufficiently control the influence of dilution water TOC and hardness on cationic polymer toxicity—A proposal to improve standardized test procedures. *Chemosphere* **2020**, *259*, 127473. https://doi.org/10.1016/j.chemosphere.2020.127473.


**Disclaimer/Publisher's Note:** The statements, opinions and data contained in all publications are solely those of the individual author(s) and contributor(s) and not of MDPI and/or the editor(s). MDPI and/or the editor(s) disclaim responsibility for any injury to people or property resulting from any ideas, methods, instructions or products referred to in the content.